malized. Form the matrix $(\xi|\xi)$ and its inverse $[\xi|\xi']$. Then

$$\sum_\eta (\xi'|\eta)[\eta|\xi] = \sum_\eta [\xi|\eta](\eta|\xi') = \delta_{\xi\xi'} . \tag{A1}$$

We expand an arbitrary function $|f)$ by computing the integrals $(f|\xi)$ and forming

$$|f) = \sum_{\xi\xi'} (f|\xi')[\xi'|\xi]|\xi) , \tag{A2}$$

an expansion which reproduces all the elements $(\xi|f)$.

If we then have an equation of the form

$$\sum_\xi A_\xi \left(\sum_\xi C_{\xi\xi}|\xi) + d_\xi|f) \right) = 0 , \tag{A3}$$

where $|f)$ is an arbitrary function, we expand f as in (A2) and substitute into (A3):

$$\sum_{\xi\xi} A_\xi \left(C_{\xi\xi}|\xi) + d_\xi \sum_{\xi'} (f|\xi')[\xi'|\xi]|\xi) \right) = 0 . \tag{A4}$$

Now act on the left-hand side with $(\eta|$, also a member of the set of functions. Then use (A1):

$$\sum_{\xi\xi} A_\xi [C_{\xi\xi}(\eta|\xi) + d_\xi(\eta|f)] = 0 . \tag{A5}$$

Now I shall identify with $|\xi)$ the combination $U_\alpha(x_1)U_\beta(x_2)$ used in the body of this paper, and with $|f)$ the quantity $\sum_k W(\Omega k\Omega')w_k(r_1r_2)U_\alpha(x_1)U_\beta(x_2)$. The quantities $C_{\xi\xi}$ arise from the action of $\mathcal{T}_\Omega(1) + \mathcal{T}_\Omega(2) + \mathcal{V}_n(1) + \mathcal{V}_n(2)$ on $U_\alpha(x_1)U_{\alpha'}(x_2)$:

$$\int_0^\infty U_\alpha(x_1)[\mathcal{T}_\Omega - \tfrac{1}{2}E]\, U_{\alpha'}(x_1)x_1^2\,dx_1 = -2(\epsilon^2/\mu)t(\alpha l_1 \alpha')(\alpha+\alpha'+2)! ,$$

$$\int_0^\infty U_\alpha(x_1)\mathcal{V}_n U_{\alpha'}(x_1)x_1^2\,dx_1 = -2\epsilon Z v(\alpha\alpha') .$$

Substitution into (A5) then gives Eq. (12).

[1]C. L. Pekeris, Phys. Rev. **126**, 11470 (1962); Phys. Rev. **115**, 1216 (1959); Phys. Rev. **112**, 1649 (1958).

[2]Charles Schwartz, Phys. Rev. **134**, A1181 (1964).

[3]Good bibliographies are given by H. A. Bethe and E. E. Salpeter [*Quantum Mechanics of One and Two Electron Atoms* (Academic, New York, 1957)] and by S. Slater [*Quantum Theory of Atomic Structure* (McGraw-Hill, New York, 1960)].

[4]B. R. Judd, *Operator Techniques in Atomic Spectroscopy* (McGraw-Hill, New York, 1963), p. 79.

[5]J. H. Bartlett, Phys. Rev. **51**, 661 (1937).

[6]V. A. Fock, Izvest. Akad. Hauk SSSR ser. Riz. **18**, 161 (1954).

[7]Charles Schwartz, Methods Comput. Phys. **2**, 241 (1963).

PHYSICAL REVIEW A VOLUME 7, NUMBER 4 APRIL 1973

Inner-Shell Ionization Cross Sections of Argon, Krypton, and Xenon by 1.5- to 5.0-MeV Protons*

Loren M. Winters, James R. Macdonald, Matt D. Brown, Louis D. Ellsworth, and Tang Chiao
Physics Department and Nuclear Science Laboratory, Kansas State University, Manhattan, Kansas 66506
(Received 27 November 1972)

The radiative decay of K-shell vacancies of argon, krypton, and xenon, and L-shell vacancies of krypton and xenon, has been observed with a Si(Li) x-ray detector for thin gas targets of these atoms excited by 1.5- to 5.0-MeV protons. X-ray yields were measured as a function of target thickness under single-collision conditions, and inner-shell ionization cross sections were determined using atomic fluorescence yields. The L-shell ionization cross sections obtained are in good agreement with theoretical calculations in the plane-wave Born approximation. The K-shell cross sections show good agreement with these calculations for the argon K shell, but fall above the theoretical values for krypton and xenon, the discrepancy with theory increasing with increasing atomic number. The binary-encounter model was also compared to the experimental K-shell ionization cross sections, and for all gases the agreement is somewhat worse. $K\beta/K\alpha$ relative intensities for krypton and xenon were determined, and good agreement of these values with the results of experiments using other modes of excitation is shown.

I. INTRODUCTION

Collisions between atoms and heavy charged particles at keV energies and above may involve considerable energy transfer between the target and projectile. This energy appears in the excitation and ionization of the collision partners, with some of the energy producing inner-shell vacancies. A number of experiments[1] have been carried out to measure the inelastic energy loss for various collision systems, and the results of these experiments have indicated the need for more information regarding the mechanism of inner-shell vacancy production. Within the last decade, a number of workers have studied this phenomenon by observing the radiative decay of inner-shell vacancies produced in collisions of energetic protons with a variety of solid targets.[2-4] In general, the ionization cross sections that have been obtained are in agreement with a theoretical model in which Coulomb excitation is assumed to be the dominant vacancy-producing mechanism. This model has been developed in the plane-wave Born approximation (PWBA) by Merzbacher and Lewis[5] as well as in the semiclassical binary-encounter approximation (BEA) by Garcia.[6] For both approximations, the ionization cross section rises steeply with projectile velocity v for $v \ll u$, the velocity of the target electron. For $v \sim u$, the cross-section curve levels off to a broad maximum and then falls off gradually for $v \gg u$. In the region of this maximum, the absolute agreement between the two results is within about 25%; however, significant differences in the energy dependence of the cross sections are predicted. For incident energies below the maximum, the BEA curve rises faster than the PWBA curve, with the former crossing over the latter just before both finally level off. Garcia[7] has indicated that the BEA fits experimental data on a variety of solid targets better than the PWBA; however, by applying corrections for Coulomb deflection of the projectile, binding of atomic electrons to the projectile, and polarization of initial atomic bound states by the projectile, Brandt *et al.*[8] have shown that the PWBA gives a good fit to their measurements of cross sections.

It should be noted that nearly all of the data referred to above are thin-target measurements. Operationally, the distinction between a thin target and a thick target is that self-absorption and stopping effects are negligible for the former. By eliminating the need to correct for these effects, the relative uncertainty in proton-induced cross sections has been reduced from about 20% for thick targets to about 5% for thin targets. In particular, the use of a thin gas target can minimize absorption and stopping effects if single-collision conditions are maintained. The motivation for this work has been to establish reliable x-ray yields for conditions of single heavy-ion-atom collisions for which stopping, charge exchange, and recoil effects may be extremely important even in thin solid targets.

In this paper we report thin-target measurements with the detailed extraction of absolute cross sections for targets of argon, krypton, and xenon in collision with protons of 1.5- to 5.0-MeV energy. X-ray-production cross sections were measured and converted to ionization cross sections by using recent experimental and theoretical values of atomic fluorescence yields. K-shell ionization cross sections were obtained for the three gases, and these were compared to both the PWBA and BEA calculations. In general, the shape of the experimental excitation function is in agreement with theory, but the absolute values of the measured cross sections agree with theory only for argon. For krypton and xenon the measured values are larger than the PWBA calculations by about 20% and a factor of 2, respectively, and the deviations with the BEA calculations are even greater. L-shell ionization cross sections were obtained only for krypton and xenon, and these are in good agreement with the PWBA calculations. The relative accuracy of the experimental cross sections was limited to 6% by alignment conditions of the gas cell and by uncertainties in the x-ray line shape due to inefficient charge collection. This made impossible a quantitative analysis of the goodness of fit of the theoretical treatments to the experimental excitation functions.

II. EXPERIMENTAL APPARATUS

Proton beams for the experiment were produced by the KSU tandem Van de Graaff accelerator and were momentum analyzed by means of a 90° bending magnet. The magnet, which was monitored by a nuclear magnetic resonance probe, provided a spread in beam energy of less than 5 keV. The absolute calibration of the magnet was determined to about 20 keV from threshold nuclear reactions. The beam was directed into the beam line by means of a switching magnet and was collimated by two sets of tantalum slits before reaching the target chamber. These slits served to define the gas-cell alignment, limit the beam current, and reduce scattering from the edges of the gas-cell apertures. The diameter of these apertures were 1.5, 2.0, 2.0, and 3.0 mm, front to rear. Beam currents of 500 nA to 1 μA through the target were typical. After passing through the gas cell, the beam was collected in a large Faraday cup (having a suppressor ring maintained at − 300 V) and was integrated by a Brookhaven current integrator.

A schematic diagram of the target chamber is shown in Fig. 1. The gas cell was differentially pumped by two 6-in. diffusion pumps, and a residual pressure of 10^{-6} to 10^{-7} torr was maintained in the beam tube. Target gas pressures were regulated by means of an MKS Baratron capacitance manometer coupled to a Granville–Phillips automatic pressure controller. The absolute accuracy of the manometer calibration was better than 10% at pressures between 1 μ and 1 torr, and the relative accuracy was considerably better. The gas was normally operated at target pressures below 10 μ to ensure thin-target conditions in the interaction region. As vibrations produced by the pressure controller considerably degraded the resolution of the x-ray detector, it was necessary to turn off the pressure regulation circuit while accumulat-

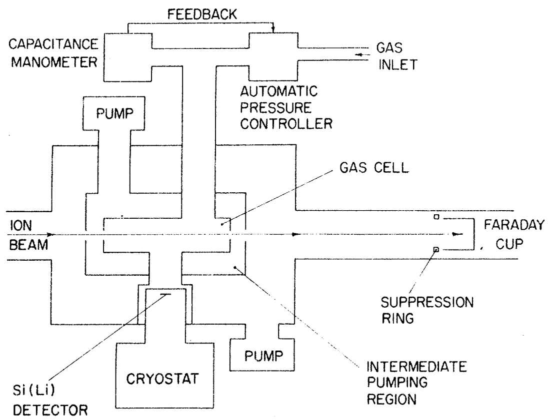

FIG. 1. Experimental apparatus used for the determination of x-ray yields from gases under proton bombardment.

ing data. Nevertheless, a precision in the pressure setting of better than 2% was maintained for all runs by continuously monitoring the pressure drift.

X rays resulting from collisions in the gas cell were detected by a liquid-nitrogen-cooled Si(Li) detector[9] mounted inside the gas cell at right angles to the beam direction. The detector, which was drifted to a depth of 3 mm, had an active area of 80 mm^2 and was maintained under separate vacuum by means of a 0.025-mm beryllium window. The detector was energy calibrated by means of a movable ^{55}Fe source mounted within the gas cell. The energy resolution was typically about 200-eV full width at half-maximum (FWHM) at 6 keV and 165-eV FWHM at 1.63 keV. The interaction region of the gas cell viewed by the detector was 1.70 cm in length and the solid angle subtended by the detector at 90° to the beam direction was 0.0136 sr. The total geometrical factor used to normalize x-ray yields was obtained by integrating the detector solid angle over the interaction length. The value used was 0.00175 cm ± 7%.

The apertures of the gas cell were made of graphite in order to minimize the continuous x-ray background due to proton bremsstrahlung. However, for proton energies above 3 MeV, a significant background was still observed. This was attributed to scattering of high-energy γ rays from nuclear reactions of ^{13}C in the apertures. The background became prohibitively large when the proton energy was above 5 MeV, in which case the inelastic scattering channel for ^{12}C contributed to the background. A characteristic x-ray background due to excitation of the stainless-steel walls of the gas cell was also observed. This background, although reduced considerably by lining the gas cell with graphite, posed a problem in the interpretation of the xenon L x-ray spectra. This will be discussed in a later section.

III. DATA NORMALIZATION AND ESTIMATED ERRORS

A. Electronic Dead Time

A pulsed optical feedback preamplifier was used with the x-ray detector and, as a result, a significant dead-time correction to x-ray yields had to be made. This was done electronically by using the amplifier gating pulse to count integrated beam current for amplifier live time only. Tests performed with an x-ray source and two amplification systems gave an accuracy of ± 2% to this correction technique even for counting rates of several thousand x rays per second for which the system dead time was over 80%. Under beam conditions of this experiment, the correction was always less than 40%, even at the highest counting rates. The beam current was reduced if necessary to satisfy this criterion. Analog-to-digital converter (ADC) dead time was also monitored in this experiment, and numerical corrections of up to 5% were made to the integrated yields to take this into account.

B. Target Thickness

The number density of gas atoms used to convert x-ray yields to single-atom yields was 3.30×10^{13} P_T atoms/cc^3, where P_T is the target pressure in microns, and where it is assumed that the deviation of the gas temperature from 20 °C is negligible. P_T is not necessarily the same as the pressure P_M indicated by the manometer, because the flow of gas through the large gas-cell apertures can cause a pressure gradient between the manometer and the cell. The following analysis of this effect provided a means of experimentally determining the magnitude of the necessary corrections to P_M.

Figure 2 is a schematic diagram of the target

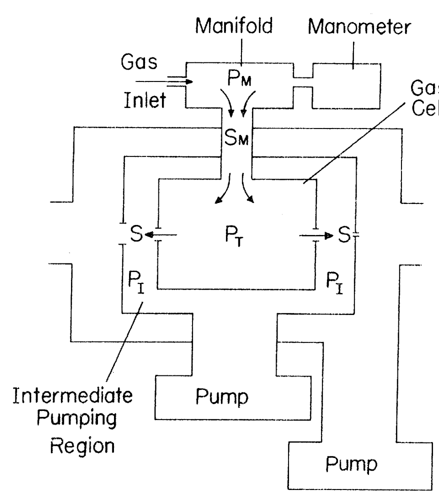

FIG. 2. Differential pumping configuration of the target chamber. Arrows indicate the general directions of gas flow.

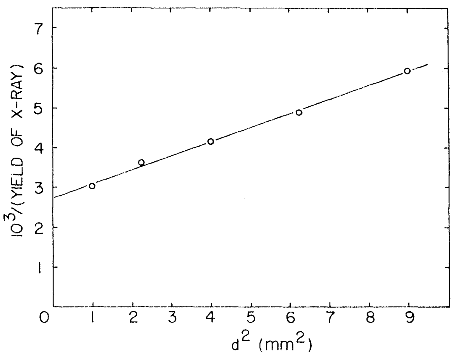

FIG. 3. Inverse of the krypton L x-ray yield as a function of the square of the gas-cell-aperture diameter d. The yield has been normalized to 1-μ manometer pressure and 1-μC collected charge. The incident proton energy is 3 MeV.

chamber with the pertinent quantities labeled. S_M is the pumping speed of unknown restrictions from manometer to cell, S is the pumping speed through each inner gas-cell aperture (assuming that apertures of the same area have the same pumping speed), and P_I is the pressure of the intermediate region. Since a 700-l/sec diffusion pump is connected directly to the intermediate region of the gas cell, it is a reasonable assumption that P_I is a well-defined pressure. Conservation of mass requires that

$$(P_M - P_T)S_M = (P_T - P_I)(2S). \quad (1)$$

To simplify Eq. (1), it is assumed that $P_I \ll P_T$ and that S is proportional to the aperture area. Equation (1) then reduces to

$$P_T = (1 + bd^2)^{-1} P_M, \quad (2)$$

where b is a gas-independent constant that must be determined.

Under thin-target conditions, the gas-cell pressure P_T is proportional to I, the observed intensity of x rays. By measuring the x-ray intensity at a number of pressures, one can experimentally determine the pressure-independent yield $Y = \Delta I/\Delta P_M$ for a given aperture diameter d. Then using Eq. (2), Y is related to d according to

$$1/Y = c(1 + bd^2), \quad (3)$$

where c is a constant which depends on the x-ray-production cross section for each gas. For five different aperture sizes ranging from $d = 1.0$ to 3.0 mm, the value of Y was measured for Ar K, Kr K, and Kr L x rays. The incident proton energy was 3.0 MeV and the beam diameter was restricted by slits to 0.5 mm in all cases. For the three lines, the value of the pressure correction, b, was extracted using a linear least-squares-fitting routine.[10] The results of the fitting procedure for Kr L x rays are shown in Fig. 3. Similar results were obtained when this procedure was carried out for the other lines. The values of b obtained in the three cases agreed to within 10%, and the mean value of b = 0.13 mm^{-2} was chosen to make the pressure correction. For the data presented in this paper d = 2.0 mm so that the following correction was applied to P_M in order to obtain P_T:

$$P_T = (0.66 \pm 0.04) P_M. \quad (4)$$

C. Absorption of X Rays and Detector Efficiency

For x rays below 5 keV in energy, absorption between source and detector is an important factor in obtaining x-ray-production cross sections. Absorption occurs in the target gas, the beryllium window, and the gold and insensitive silicon layers of the detector. Self-absorption in the gas targets is negligible and amounts to less than 0.01% (as determined from mass absorption coefficients of Storm and Israel[11]) for all the x rays observed in this experiment. However, absorption in the remaining three layers must be taken into account in determining detector efficiency and absolute cross sections.

Published experimental efficiency curves for Si(Li) detectors have been obtained[12,13]; but, these do not cover the energy region of the lines observed in this work. This lack of absolute efficiency standards is a fundamental problem which has not been solved for low-energy x-ray detectors in general. The experimental uncertainties associated with the higher-energy efficiency curves suggest that a theoretical calculation may be as accurate at the present time. The problem with this type of calculation is that the thicknesses of the absorbing layers, in particular the gold and silicon layers, are not well known, and one must use manufacturer specifications for the purity and thickness of the beryllium window. Nevertheless, a reasonable estimate of the efficiency can be obtained when absorption due to the gold and silicon layers is small. This method has been used to compute an efficiency curve for the detector. Such a curve has also been calculated by Marrus and Schmieder[14] for a windowless Si(Li) detector in the energy region below 5 keV.

To compute the efficiency curve, we used the following thicknesses: 0.025-mm ± 20% Be, a dead layer equivalent of 0.1-μ Si at 6 keV as estimated by the detector manufacturer,[9] and an average 20-μg/cm^2 Au. Absorption coefficients were taken from the work of Storm and Israel.[11] The results are plotted in Fig. 4 along with separate absorption curves for each of the three layers. At energies below 2 keV, absorption in the beryllium window dominates, and the correction can be estimated to about 20% accuracy from the thickness specifica-

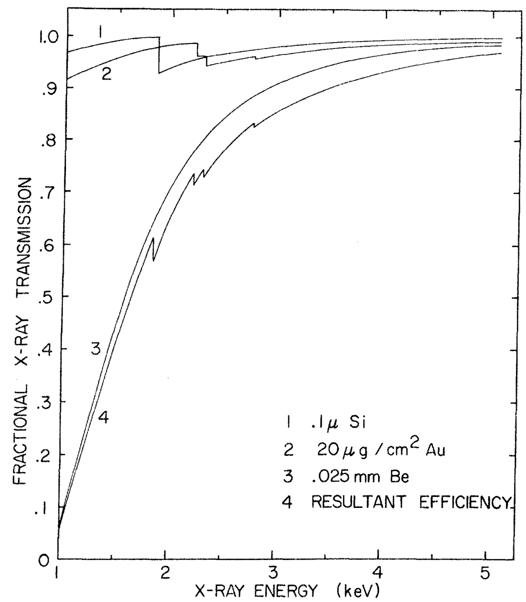

FIG. 4. X-ray absorption curves for the Be window, the gold layer, and the dead silicon layer of the Si(Li) detector. The total efficiency curve of the detector for x rays below 5 keV is also shown.

tions supplied by the manufacturer. For krypton L x rays, the efficiency is estimated to be $49\pm10\%$. For x rays near 3 keV, the absorption is comparable for all three layers. The correction here can be estimated to an accuracy of only 50% because of the uncertainty in the thickness of the gold layer. For argon K x rays, the estimated efficiency is $85\pm7\%$ and for xenon L x rays it is $95\pm2\%$. Since the xenon L x-ray spectrum extends over a wide energy range (3.7–5.3 keV), the latter efficiency was obtained by weighting the efficiency for each resolved peak of the spectrum by the intensity of that peak. This should be a valid procedure since the calculated detector efficiency only varies from 92 to 97% over this energy range.

The efficiencies used for the x rays greater than 10 keV are determined from the effective absorption in the active depth of the detector. For the K x rays of krypton and xenon the following efficiencies were taken from a theoretical curve supplied by the manufacturer: Kr $K\alpha$, 100%; Kr $K\beta$, 100%; Xe $K\alpha$, 51%; Xe $K\beta$, 41%.

A fact which may affect the detector efficiency is the existence of impurities in or on the Be window. This possible source of systematic error has not been included in the results of this experiment.

D. Beam Transmission

A critical factor in obtaining x-ray yields in gas targets is to have 100% beam transmission through the gas cell. If, owing to improper aperture alignment or beam-focusing conditions, the Faraday cup does not collect all particles which pass through the interaction region, then the experimental cross sections will be too large. This problem should be greatest at low proton energies where good beam focusing is most difficult to obtain and should improve as the proton energy increases. Thus, a relative error, which decreases as beam energy increases, may be introduced into the cross sections for a given x-ray line.

In order to examine this possible error systematically, we have taken duplicate sets of data for argon K, krypton L, and krypton K x rays for beam energies from 1.5 to 4.5 MeV. These two sets were taken on different days so that alignment and beam-focusing conditions could be expected to be different for the two runs. It was indeed observed that for a given x-ray line, the energy dependence of the x-ray yields was slightly different for the two sets of data. In particular, if smooth curves were drawn through both sets of data for argon K x rays, the ratio of x-ray yields between the two curves at a given collision energy varied linearly from 0.813 at 2 MeV to 0.884 at 4.5 MeV. This result is shown by the circles in Fig. 5. It should be noted that the ratio at 1.5 MeV falls considerably below the straight line joining the other points. This may be indicative of the difficulty in focusing the beam through the gas cell at this energy.

For the data set which gave higher x-ray yields, we have analyzed the effect of incomplete beam transmission by making discrete changes in the gas-cell-aperture alignment and mapping out deviations of the argon K x-ray yield from its minimum value. This minimum was assumed to occur for conditions of 100% beam transmission through the gas cell when the proton beam was restricted

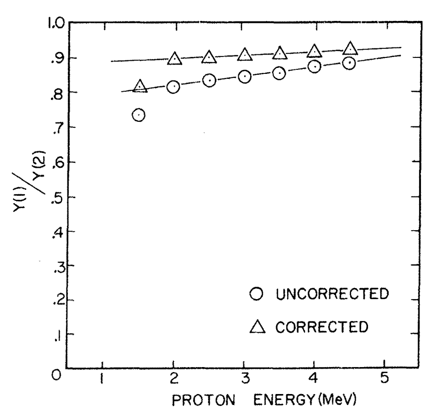

FIG. 5. Comparison of argon K x-ray yields [$Y(1)$ and $Y(2)$] measured on two separate days. The ratio $Y(1)/Y(2)$ is plotted as a function of incident proton energy for the raw data (circles) as well as for the data with a correction applied for incomplete beam transmission (triangles).

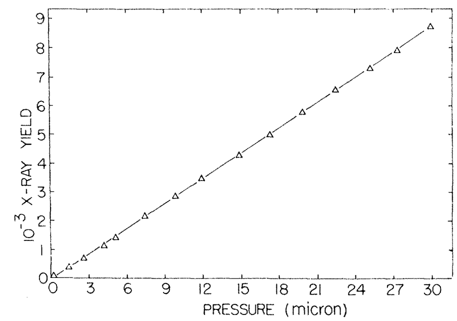

FIG. 6. Yield of Kr L x rays vs manometer pressure. The yields are normalized to a constant value of collected charge, and the incident proton energy is 3 MeV.

in diameter by the beam line slits. In this way, corrections to previously determined x-ray yields at 2 and 4 MeV were obtained. By assuming a linear relationship between the magnitude of the correction and the collision energy, a correction factor for incomplete beam transmission at each collision energy was determined. These corrections varied from 0.91 at 1.5 MeV to 0.97 at 5.0 MeV.

When the corrections are applied to the data, the x-ray-yield ratios indicated by the triangles in Fig. 5 were obtained. These indicate that the correction technique has made the energy dependences for the two sets of data more nearly consistent with each other, the deviation of the ratios from a constant value being only about 3% over the energy range of 2 to 4.5 MeV. An average discrepancy of about 10% in absolute yields still exists at all incident energies (except at 1.5 MeV, where it is 20% but this may be the result of unavoidable changes in operating conditions such as the absolute determination of solid angle from one run to the next. The corrections determined above were also applied to the krypton and xenon x-ray yields which were taken under the same conditions as the argon K x-ray data. Where applicable, the corrected set of data was averaged with the duplicate set in order to obtain values from which to calculate cross sections. In applying this correction to account for inefficient beam collection we have obtained a weighted average of duplicate data sets with the lower set of data weighted as the better of the two.

The use of the above procedure is believed to reduce the relative error due to possible misalignment of the gas cell, and the absolute uncertainty in the data caused by incomplete beam collection is estimated to be less than 10%.

IV. DATA ANALYSIS

A. Extraction of Yields

For each target gas at each energy, x-ray yields were measured for at least five different target thicknesses with manometer pressures from 0 to 10 μ. At these pressures, and even up to pressures of 30 μ, the growth of the x-ray yield with manometer pressure was strictly linear, effectively ensuring single-collision conditions. This is illustrated in Fig. 6 in which the yield of krypton L x rays resulting from 3-MeV proton bombardment is plotted as a function of manometer pressure.

The experimental points for each target gas and beam energy were fitted by a linear least-squares routine[10] to obtain the yield of x rays per micron of pressure recorded on the manometer. By using this procedure, errors resulting from statistical uncertainty in the x-ray counts and relative uncertainty in the target thickness were less than 2% for krypton L, xenon L, and argon K x-ray yields and less than 5% for krypton K and xenon K x-ray yields.

Sample spectra obtained on the TMC multichannel analyzer for argon and krypton x-ray lines are shown in Fig. 7. The procedure used to obtain x-ray yields from such spectra was to set markers on either side of the x-ray peaks at the points where the peaks merged into the background and then to sum the counts channel by channel between the markers. For argon, no attempt was made to resolve the $K\alpha$ and $K\beta$ peaks for purposes of integration. In the case of krypton, however, the $K\alpha$ and $K\beta$ peaks were well resolved so that the peaks could be integrated separately in order to obtain $K\beta/K\alpha$ relative intensities. The krypton L x-ray peak showed no signs of structure and no effort was made to extract separate lines from the data.

Integration of the xenon L x-ray spectrum was complicated by the existence of background x rays resulting from excitation of the stainless-steel walls of the gas cell. In particular, the Cr $K\alpha$ line (5.411 keV) overlapped the xenon $L\gamma_{2,3}$ peak. This is shown in Fig. 8(b) at an incident proton energy of 4.5 MeV. For comparison, Fig. 8(a) shows the xenon L x-ray spectrum at an incident proton energy of 2 MeV for which the background peaks are too weak to be observed. To correct for this background, an analysis was made of the spectra obtained in proton bombardment of argon targets. For these spectra, the background peaks were well separated from the Ar K line so that the Cr $K\alpha$ and Fe $K\alpha$ peaks could be integrated and their relative intensities determined. After obtaining average relative intensities $[K\alpha(\mathrm{Cr})/K\alpha(\mathrm{Fe})]$ at each energy, these ratios were multiplied by the $K\alpha$(Fe) yields for each xenon spectrum to obtain the corresponding $K\alpha$(Cr) yields. For incident energies below 3.5 MeV, the background correction was negligible; however, for higher incident energies the correction amounted to 1 to 4% of the total xenon L x-ray yield. The uncertainty in this correction technique is estimated to be less than 5%.

For all the x-ray lines except the xenon K lines, large peak-to-background ratios were maintained.

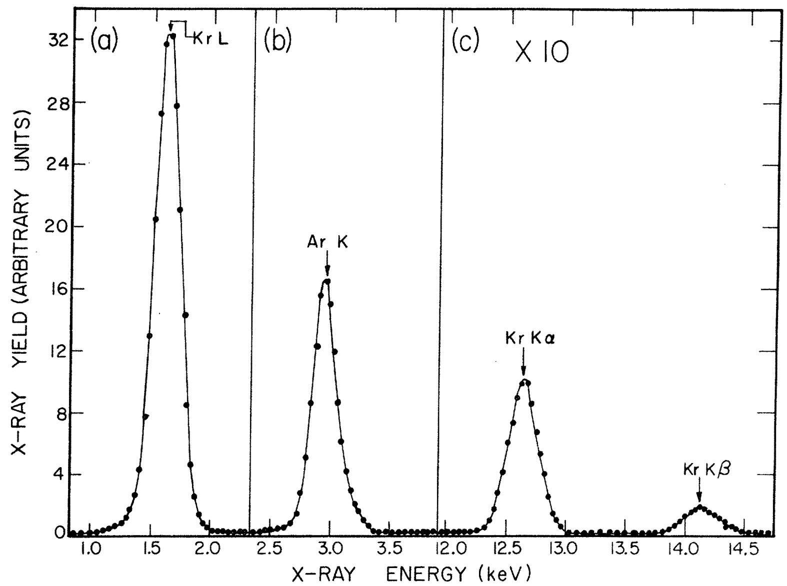

FIG. 7. Pulse-height spectra for the (a) Kr L, (b) Ar K, and (c) Kr K x-ray lines. For all spectra, the incident proton energy is 3.5 MeV and the manometer pressure is 10 μ.

These ratios varied from 50 : 1 at the lowest proton energies to 100 : 1 at the higher energies. For this reason, it was unnecessary to make background corrections to x-ray yields prior to application of the linear fitting procedure to the data taken at a number of different target pressures. This procedure then corrected automatically for the pressure-independent background component. For the low-intensity xenon K x rays, on the other hand, the background was a major consideration (see Fig. 9). For all xenon K x-ray spectra, peak-to-background ratios never exceeded 4 : 1; consequently, linear background was subtracted from all x-ray yields prior to the application of the fitting routine for the different target thicknesses.

In addition to the pressure-independent background, a pressure-dependent background was exhibited on the low-energy side of all x-ray lines except the xenon K lines, for which the effect was too small to observe. Slivinsky and Ebert[15] have reported a tailing behavior of x-ray lines detected by a Si(Li) detector, and they have attributed this to inefficient charge collection in the detector. The following factors suggest that for our data the pressure-dependent tailing to a large extent represents real x-ray events reduced from the full-energy peak

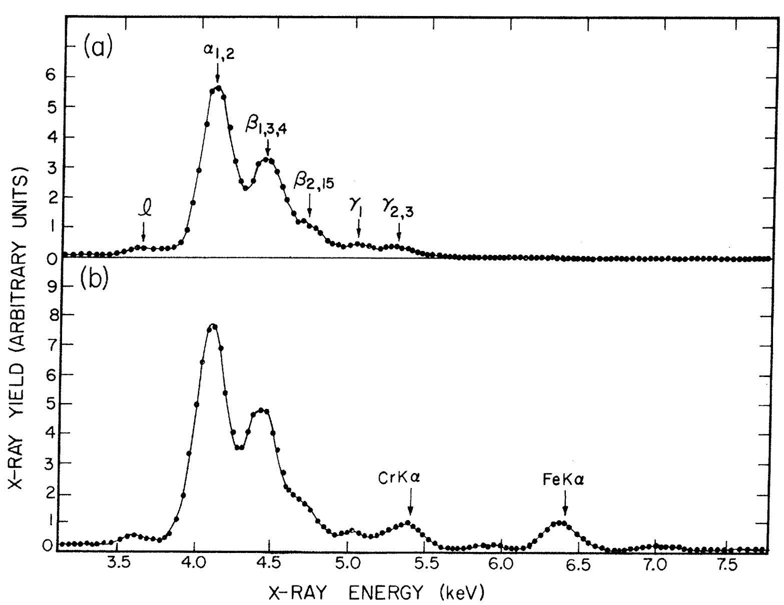

FIG. 8. Pulse-height spectra for the xenon L x-ray lines at incident proton energies of (a) 2 MeV and (b) 4.5 MeV.

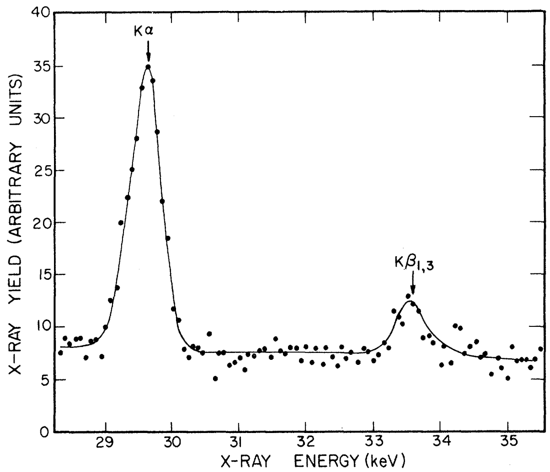

FIG. 9. Pulse-height spectra for the xenon $K\alpha$ and $K\beta$ x-ray lines for 5-MeV proton bombardment.

and related to phenomena in the Si(Li) detector: (i) Variations in beam focusing and gas-cell-alignment conditions do not affect the counts in the tail relative to the peak, while the pressure-independent background may change radically as a result of enhanced slit-edge scattering. (ii) The intensity of the tail shows the same dependence on incident proton energy as the corresponding x-ray line. (iii) The spectrum of an ^{55}Fe x-ray source also exhibits such a tail, with the relative intensity of the tail dependent upon operating parameters such as threshold levels and gain. In all cases, this amounted to less than 15% of the pressure-normalized x-ray yields. Restricting the x rays entering the detector with a collimator did not significantly reduce the tail without severely reducing the detector area. However, with the same gas-cell detector geometry, the contribution of the tail to the pressure-normalized yields of an x-ray line differed by as much as 30% on different runs. This was true for both Ar K and Kr L x-ray lines and suggests that detector operating conditions may be a contributing factor to the discrepancy (see note added in proof).

In light of these considerations, the x-ray yields that we have used to calculate x-ray-production cross sections include contributions from the pressure-dependent tail for the argon K, krypton L, and xenon L lines. For the krypton K lines, much of the tail was obscured by background peaks of lower energy and was not fully included in the yields. Clearly, the position of the low-energy cutoff of the detector will affect the x-ray yields as determined above. Extending the tail linearly to zero x-ray energy results in no more than a 5% increase in cross sections. It is clear that a better understanding of the spectral response of Si(Li) detectors is necessary before absolute yields can be determined to better accuracy with these devices.

B. Calculation of Cross Sections

X-ray-production cross sections were calculated from x-ray yields according to the thin-target formula,

$$\sigma_x = \frac{I}{N n_i \epsilon (L\Omega/4\pi)}\,, \tag{5}$$

where I is the x-ray yield corrected for electronic dead time and pressure gradient, N is the number of target atoms per unit volume, n_i is the number of incident protons, ϵ is the detector efficiency for the particular x-ray line, and $L\Omega$ is the solid angle integrated over the interaction length viewed by the detector.

Ionization cross sections were obtained by dividing the x-ray cross section by the fluorescence yield. K-shell fluorescence yields used were taken from a table of "most reliable" values compiled by Bambynek *et al.*[16] These were 0.122 for argon, 0.666 for krypton, and 0.894 for xenon. Fluorescence yields used for the L shell were 0.0241 for krypton from theoretical calculations of McGuire[17] and 0.11 ± 0.01 for xenon reported by Bambynek *et al.*[16] from the experimental work of Hohmuth and Winter.[18] The krypton L-shell fluorescence yield has been corrected for Coster–Kronig yields, also calculated by McGuire.[17] Experimental L-shell fluorescence yields for xenon show agreement of better than 10% with theoretical L-shell results.[16] Although no recent measurements of the krypton L-shell fluorescence yield exist for comparison with theory, it is not believed that the choice of fluorescence yield contributes substantially to the uncertainty in the reported ionization cross sections.

C. Error Analysis

For all the x-ray lines studied, contributions to the absolute uncertainty in the yield are estimated as the following: 10% from the manometer calibration, 7% from the interaction length and solid-angle integration, 7% from the target thickness correction for the pressure gradient in the gas cell, and 10% from corrections for incomplete beam transmission. In addition, the data-analysis procedure contributes a 7% uncertainty for the Kr L, Ar K, and Xe L lines and a 10% uncertainty for the Kr K and Xe K lines. This latter source of uncertainty includes statistical errors as well as errors due to pressure fluctuations and spectrum integration procedures. Uncertainty in cross sections due to detector efficiency is estimated to be 10% for Kr L, 7% for Ar K, 2% for Xe L, 10% for Xe K, and negligible for Kr K x rays. No estimate of uncertainty has been made for impurities in or on the Be window of the detector. If this systematic er-

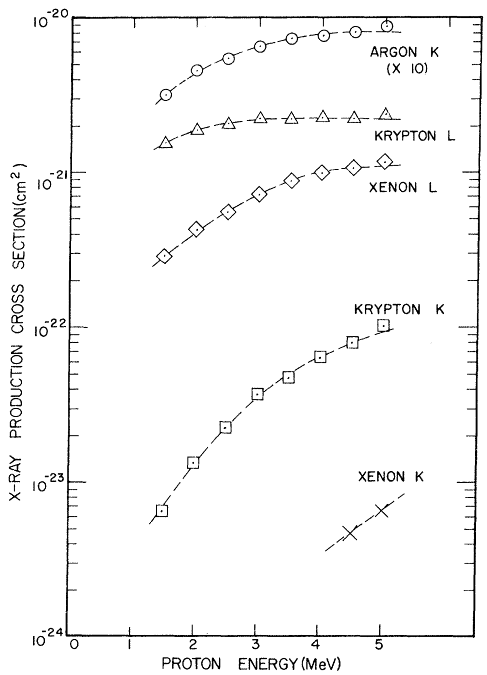

FIG. 10. Experimental x-ray-production cross sections (in units of cm^2/atom/proton) as a function of incident proton energy for argon, krypton, and xenon targets. The relative uncertainty in the data is given approximately by the size of the symbol.

ror is significant, then the reported cross sections are too small.

The above uncertainties result from corrections that have been included in the data analysis. A total uncertainty in the x-ray-production cross section is obtained by adding the uncertainties in quadrature. (It should be noted that the uncertainty in beam transmission is omitted from this procedure since incomplete beam transmission can only serve to raise the x-ray yields above some minimum value. This source of systematic error is estimated to contribute an uncertainty of less than 10% in the direction of decreasing cross section.) This amounts to about 17% for all the x-ray lines studied. In cases where independent sets of data from different runs for a given line have been averaged together (Ar K, Kr L, Kr K at 1.5 to 4.5 MeV), the absolute uncertainty is reduced to about 14%.

The relative uncertainty between cross sections at different proton energies for a given line is considerably less than the absolute uncertainty since the only contributions to the former are from beam transmission and analysis of x-ray yields. For all the x-ray lines studied, the relative uncertainty is estimated at 6%. This estimate is borne out by a typical scatter of 5% in the data points from a smooth dependence of x-ray-production cross section as a function of collision energy (Fig. 10). Although this uncertainty is small enough to allow a qualitative comparison between the ability of the PWBA and BEA calculations to fit the experimental data, it is believed possible to reduce the uncertainty to a few percent with a better analysis of beam normalization through the gas target and a more detailed understanding of the detector response function.

V. RESULTS AND DISCUSSIONS

A. Cross Sections

We have measured x-ray-production cross sections for K x rays of argon, krypton, and xenon and L x rays of krypton and xenon under proton bombardment. These cross section are plotted in Fig. 10 as a function of the incident proton energy. A summary of the x-ray-production and ionization cross sections is given in Table I. Where applicable, the contribution of the spectrum tail and the pressure-dependent background of the x-ray peak to the cross section is given in parentheses.

K-shell ionization cross sections determined from these results are shown in Fig. 11 for argon and Fig. 12 for krypton and xenon. Also shown are the theoretical results of the PWBA (solid line) and BEA (dashed line) treatments. The scaling of the data by K-shell binding energy I_K is the same as that used by Garcia.[6] The argon data lie near the peak of the excitation function in the region where the BEA curve crosses and goes above the PWBA curve. Absolute agreement of the experi-

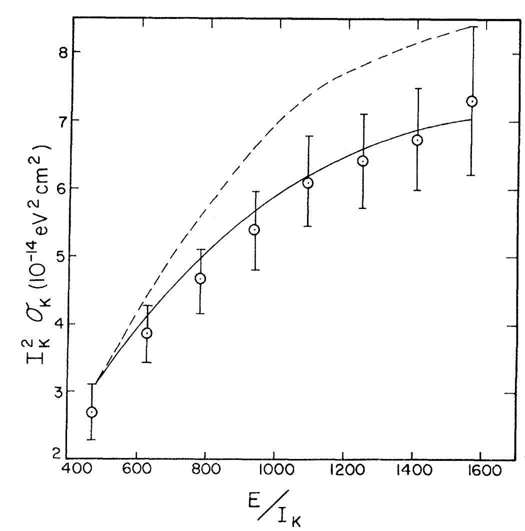

FIG. 11. K-shell ionization cross sections for argon. The cross section σ_K is scaled by the square of the binding energy I_K of an argon K-shell electron, and the collision energy E is scaled by the inverse of this quantity. The solid line is the PWBA result (Ref. 21) and the dashed line is the BEA result (Ref. 7). The absolute uncertainty in the data is indicated by the error bars.

TABLE I. X-ray-production and ionization cross sections.

Collision energy (MeV)	X-ray-production cross section (barns) Ar K	Kr K	Xe K	Kr L	Xe L	Ionization cross section (barns) Ar K	Kr K	Xe K	Kr L	Xe L
1.5	319	6.23		1570	290					
	(11.8)[a]	(5.7)		(4.2)	(14.6)	2610	9.35		66000	2640
2.0	457	13.2		1880	430					
	(11.8)	(3.4)		(2.8)	(13.5)	3750	19.8		79300	3910
2.5	553	22.5		2040	558					
	(12.5)	(4.7)		(4.2)	(12.4)	4530	33.8		86200	5070
3.0	638	36.6		2220	678					
	(12.2)	(5.2)		(5.4)	(13.8)	5230	55.0		93800	6160
3.5	725	47.4		2190	869					
	(12.0)	(5.3)		(4.5)	(12.5)	5940	71.2		92300	7900
4.0	761	63.8		2230	979					
	(13.8)	(4.6)		(4.9)	(12.7)	6240	95.8		94100	8900
4.5	799	79.2	4.73	2220	1046					
	(12.7)	(5.2)		(4.6)	(12.6)	6550	119	5.29	93700	9510
5.0	868	102	6.64	2330	1154					
	(9.2)	(6.6)		(4.2)	(12.9)	7110	153	7.43	98500	10500

[a]Where applicable, the contribution of the pressure-dependent background yield to the x-ray-production cross section is given in parentheses under the cross section.

mental data with the PWBA is good; however, the BEA curve lies slightly above the limits of absolute error indicated by the error bars. For krypton and xenon, the data lie in the region where both the BEA and PWBA are rising steeply with collision energy, corresponding to the incident proton velocity being considerably less than the mean velocity of the K-shell electron. Neither theoretical treatment fits the experimental results for krypton and xenon, the data being consistently higher than the PWBA, which is above the BEA in this region. In fact, for all the experimental K-shell ionization cross sections, agreement with the theoretical calculations becomes progressively worse as the atomic number of the target increases. Whereas the argon data show good agreement with the PWBA, the krypton data are about 30% greater, and the xenon data are over twice as large. A possible explanation of this trend is that relativistic effects, which are ignored by both the PWBA and BEA calculations, may be increasingly important for the tightly bound krypton and xenon K-shell electrons. It should be noted, however, that initial-[8] and final-[19] state polarization of the target electron may also contribute to the observed discrepancy above theory. A quantitative analysis of such effects has not been made in this paper.

Our experimental L-shell ionization cross sections are plotted in Fig. 13 for krypton and Fig. 14 for xenon. Also shown are the results of the PWBA calculations. The scaling is that of Merzbacher and Lewis,[5] the abscissa being the dimensionless energy parameter

$$\eta_L = \frac{(m/M)(E/E_R)}{Z_L^2}, \tag{6}$$

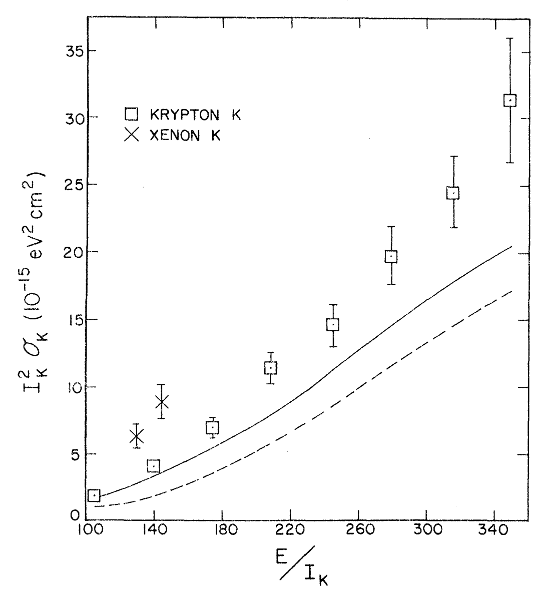

FIG. 12. K-shell ionization cross sections for krypton and xenon. The cross section σ_K is scaled by the square of the binding energy I_K of a K-shell electron of the target atom, and the collision energy E is scaled by the inverse of this quantity. The solid line is the PWBA result (Ref. 21) while the dashed line is the BEA result (Ref. 7). The error bars indicate the absolute uncertainty in the data.

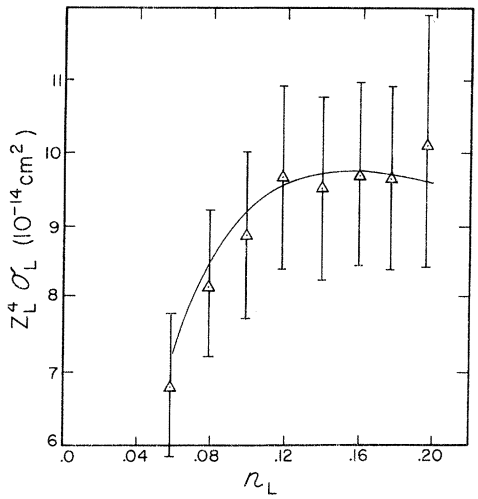

FIG. 13. L-shell ionization cross sections for krypton as a function of the dimensionless energy parameter η_L. The cross section σ_L is scaled by the fourth power of the screened nuclear charge Z_L seen by an L-shell electron. The solid line is the result of PWBA calculations (Ref. 21). The absolute uncertainty of the data is indicated by the size of the error bars.

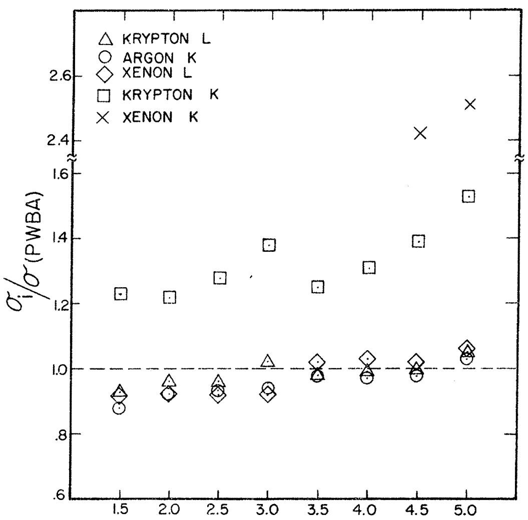

FIG. 15. Comparison of experimental ionization cross sections to PWBA calculations (Ref. 21). The ratio of the experimental cross section σ_i to the calculated cross section σ(PWBA) is plotted against the incident proton energy.

where m/M is the ratio of electron to proton mass, E/E_R is the collision energy in rydbergs, and $Z_L = Z - 4.15$ is the screened nuclear charge seen by an L-shell electron.[20] For krypton, the data lie on the peak of the excitation function, whereas for xenon the energy range of this experiment is on the low-energy side of the peak. In both cases, absolute agreement with the PWBA is excellent as is the relative shape of the excitation function.

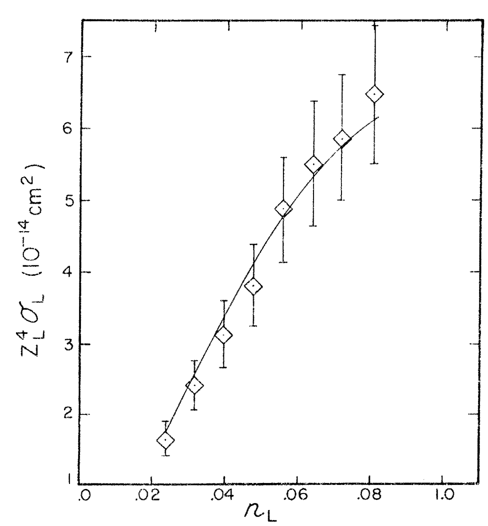

FIG. 14. L-shell ionization cross sections for xenon as a function of the dimensionless energy parameter η_L. The cross section σ_L is scaled by the fourth power of the screened nuclear charge Z_L seen by an L-shell electron. The solid line is the result of PWBA calculations (Ref. 21). The absolute uncertainty of the data is indicated by the size of the error bars.

In order to compare the energy dependence of the experimental ionization cross sections with theory[7,21] we have plotted the ratios σ_i/σ(BEA) and σ_i/σ(PWBA), as a function of the incident proton energy where σ_i is the experimental ionization cross section and σ(PWBA) and σ(BEA) are the corresponding theoretical ionization cross sections. For the PWBA ratios shown in Fig. 15, the argon K-, krypton L-, and xenon L-shell data all cluster about the constant value $\sigma_i/\sigma(\text{PWBA}) = 1$. These data do exhibit a slight upward trend with proton energy; however, within the relative uncertainty of the data, the energy dependence of the experimental cross sections is in reasonable agreement with the PWBA theory. As shown in Fig. 16, the ratios of argon K-shell ionization cross sections to BEA cross sections show a decreasing trend at the lower energies and an increasing trend at higher energies, although the trends are only slightly outside relative uncertainty in the data. This points up the difference in energy dependence of the two theoretical treatments, but these trends are not sufficiently large to say that the energy dependence of the data favors one treatment over the other.

For the krypton K-shell cross-section ratios, much more striking trends are observed. The σ_i/σ(PWBA) ratios (Fig. 15) clearly show a rising trend with proton energy, while the reverse is true

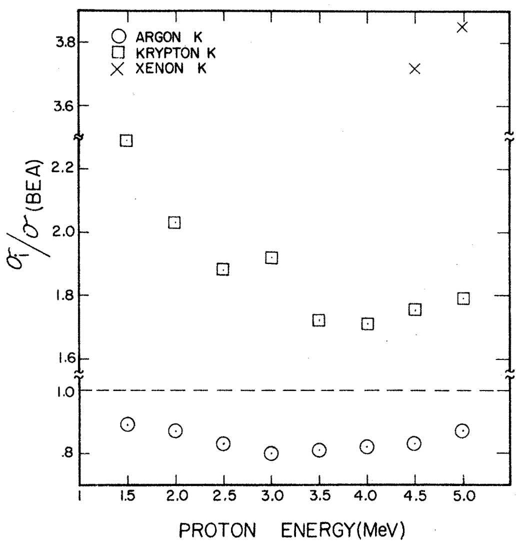

FIG. 16. Comparison of experimental ionization cross sections to BEA calculations (Ref. 6). The ratio of the experimental cross section σ_i to the calculated cross section σ(BEA) is plotted against the incident proton energy.

for the σ_i/σ(BEA) ratios (Fig. 16). Over the energy range of this experiment the ratios change by as much as 20% for the PWBA and 30% for the BEA. Neither theory gives a good fit to the data over the full energy interval; however, for energies below about 3.0 or 3.5 MeV, the PWBA seems to give the better fit whereas above these energies both treatments are consistent with the observed dependence.

For the xenon K-shell ionization, no gross differences in the deviation of cross-section ratios from unity can be observed for the two data points for either the PWBA or BEA treatments. We do not have enough data on the line to make further comparison of the energy dependence, but one should note that the approximate factor-of-3 underestimate of the cross section in both treatments is far outside experimental errors.

B. Relative Intensities ($K\beta/K\alpha$)

Ratios of $K\beta$ to $K\alpha$ x-ray yields were obtained for krypton and xenon. Pressure-dependent background contributions were subtracted from the yields; in addition, the yields were corrected for differences in detector efficiency for the $K\alpha$ and $K\beta$ energies. Averaging the $K\beta/K\alpha$ ratios for all the experiments gives mean values of 0.189 ± 0.010 for krypton and 0.225 ± 0.025 for xenon. No systematic trends of the ratios with collision energy were observed.

Hansen *et al.*[22] have measured the $K\beta/K\alpha$ ratios for krypton and xenon using carrier-free radioactive sources. Their results are 0.1634 for krypton and 0.2345 for xenon. Using fluorescence excitation, Slivinsky and Ebert[15] have also determined the $K\beta/K\alpha$ ratio for krypton, obtaining a value of 0.1715. Although the deviations of these values from our value for krypton are slightly greater than experimental uncertainty, the agreement for both gases is considered good.

VI. SUMMARY

We have observed the K- and L-shell x-ray production in collisions of argon, krypton, and xenon atoms with protons at MeV energies as a means of obtaining inner-shell ionization cross sections for these atoms. The experimental L-shell ionization cross sections for xenon and krypton and K-shell ionization cross sections for argon show good agreement—both in absolute magnitude and energy dependence—with the plane-wave Born approximation calculations of Merzbacher and Lewis.[5] The K-shell ionization cross sections for krypton and xenon, however, are larger than the PWBA results, the disagreement being considerably greater for xenon. These K-shell ionization cross sections were also compared with the binary-encounter model of Garcia,[6] with similar results being obtained. In addition, discrepancies with the BEA were observed for the magnitude of the argon K-shell ionization although the energy dependence of these cross sections agreed favorably with BEA calculations.

For krypton and xenon, $K\beta/K\alpha$ relative intensities were determined. Agreement of these values with the results of experiments[15,22] using other modes of excitation is good.

Note added in proof. A detailed discussion of the tailing behavior of Si(Li) detectors is given by H. U. Freund, J. S. Hansen, E. Karttunen, and R. W. Fink, in *Radioactivity in Nuclear Spectroscopy*, edited by J. H. Hamilton (Gordon and Breach, New York, 1972), Vol. 2, p. 623, and Nucl. Instrum. Methods 106 (1972).

*Work partially supported by the U. S. Atomic Energy Commission under Contract No. AT(11-1)-2130.

[1]A summary of experiments involving the measurement of inelastic energy loss for a variety of collision systems is given by Q. C. Kessel, in *Case Studies in Atomic Collision Physics,* edited by E. W. McDaniel and M. R. C. McDowell (North-Holland, New York, 1969), Vol. 1, p. 412.

[2]J. M. Khan, D. L. Potter, and R. D. Worley, Phys. Rev. **145**, 23 (1966).

[3]R. R. Hart, F. William Reuter III, H. P. Smith, Jr., and J. M. Khan, Phys. Rev. **179**, 4 (1969).

[4]A partial summary of experiments involving the measurement of ionization cross sections for ion-atom collisions is given by J. Lin, J. L. Duggan, and R. F. Carlton, in *Inner Shell Ionization Phenomena and Future Applications*, edited by R. W. Fink, S. T. Manson, J. M. Palms, and P. V. Rao (U. S. Atomic Energy Commission Report Conf. No. 720404, 1973), p. 998.

[5]E. Merzbacher and H. W. Lewis, in *Encyclopedia of Physics*, edited by S. Flügge (Springer-Verlag, Berlin, 1958), Vol. 34, p. 166.
[6]J. D. Garcia, Phys. Rev. A **1**, 280 (1970).
[7]J. D. Garcia, Phys. Rev. A **1**, 1402 (1970).
[8]W. Brandt, in *Inner Shell Ionization Phenomena and Future Applications*, edited by R. W. Fink, S. T. Manson, J. M. Palms, and P. V. Rao (U. S. Atomic Energy Commision Report Conf. No. 720404, 1973), p. 948.
[9]Kevex Corporation, Burlingame, Calif.
[10]The Hewlett-Packard Calculator, model 9100B, Program Library.
[11]E. Storm and H. I. Israel, Nucl. Data A **7**, 565 (1970).
[12]R. L. Watson, L. W. Lewis, and J. B. Natowitz, Nucl. Phys. A. **154**, 561 (1970).
[13]R. J. Gehrke and R. A. Lokken, Nucl. Instrum. Methods **97**, 219 (1971).
[14]R. Marrus and R. W. Schmieder, Phys. Rev. A **5**, 1160 (1972).
[15]V. W. Slivinsky and P. J. Ebert, Phys. Rev. A **5**, 1581 (1972).
[16]W. Bambynek, B. Crasemann, R. W. Fink, H. U. Freund, H. Mark, C. D. Swift, R. E. Price, and P. V. Rao, Rev. Mod. Phys. **44**, 716 (1972).
[17]E. J. McGuire, Phys. Rev. A **3**, 587 (1971).
[18]K. Hohmuth and G. Winter, Phys. Lett. **10**, 58 (1964).
[19]J. H. McGuire (private communication).
[20]J. C. Slater, Phys. Rev. **36**, 57 (1930).
[21]G. S. Khandelwal, B. H. Choi, and E. Merzbacher, At. Data 1, 103 (1969).
[22]J. S. Hansen, H. U. Freund, and R. W. Fink, Nucl. Phys. A **142**, 604 (1970).

PHYSICAL REVIEW A VOLUME 7, NUMBER 4 APRIL 1973

Properties of Resonance Wave Functions*

Richard M. More and Edward Gerjuoy
Department of Physics, University of Pittsburgh, Pittsburgh, Pennsylvania 15213
(Received 12 December 1972)

Resonances of quantum systems are associated with poles of the Green's function which occur at complex energies. The wave functions corresponding to such poles increase exponentially at large distances and so are very badly divergent. Nevertheless, these resonance wave functions have useful properties which can be exploited in cases where only their behavior at small distances is relevant. In this paper we construct and study such resonance wave functions for several illustrative quantum systems of theoretical interest. It is shown that the wave functions may be considered *renormalized* in a sense analogous to that of quantum field theory. However, the renormalization which occurs here is entirely automatic and the theory has neither *ad hoc* procedures nor infinite quantities. In addition to other results, we obtain a representation of the Green's function in terms of the resonance wave functions; this representation appears likely to be useful because it has an energy dependence that is especially simple.

I. INTRODUCTION

There is an enormous literature dealing with resonances of quantum systems, and usually the resonances are described via continuum (scattering) theory. However, this description seems to miss the most striking characteristic of a narrow resonance. A narrow scattering resonance is always associated with a long-lived decaying state, a state which physically resembles a true discrete eigenstate. The resemblance is especially strong when the lifetime is long. Obviously one should choose a description in which this resemblance is clearly exhibited and emphasized. To this end it appears profitable to introduce and study a set of resonance wave functions.

With these wave functions (one for each resonance) we can see the general physical similarity of resonance states and bound states, and also the specific technical differences. The resonance wave functions will necessarily have some abnormal or anomalous properties which reflect the time dependence of the decaying state.

In this paper we have constructed and studied resonance wave functions for several illustrative models of theoretical interest. The definition of these wave functions was suggested by a perturbation theory of decaying states.[1-4] The most stubborn abnormality is their refusal to be normalized or mutually orthogonal. In fact we shall find that the resonance wave functions are *renormalized* in a sense described below. However, this renormalization is entirely automatic (there is no *ad hoc* step in the mathematics) and the theory has no infinite quantities. Actually, both renormalized and also nonrenormalized perturbation theories exist and are correct; they differ because they calculate different quantities. The situation is thus much simpler than the renormalization of quantum field theories.

The main object of this paper is then to identify and interpret the anomalous normalization properties of the resonance wave functions. The normalization is not at all arbitrary, but proves to have a definite physical significance. This interpretation is given in Sec. II.